ELSEVIER

Journal of Nuclear Materials 266–269 (1999) 1051–1058

journal of nuclear materials

# FT-IR studies of graphite after keV-energy hydrogen ion irradiation

Yoshitaka Gotoh [a,*], Soji Kajiura [b]

[a] *Hitachi Research Laboratory, Hitachi Ltd., 1-1 Saiwai-cho, 3-chome, Hitachi-shi, Ibaraki-ken 317, Japan*
[b] *Hitachi Works, Hitachi Ltd., 1-1 Saiwai-cho, 3-chome, Hitachi-shi, Ibaraki-ken 317, Japan*

**Abstract**

Fourier-transform infrared absorption spectroscopy (FT-IR) studies were made on vapor-grown carbon fiber (VGCF) after successive irradiations of 6, 3 and 1 keV-$H^+$ to saturation at 373–923 K, and after the irradiations at 623 K followed by a heat-treatment at 893–1150 K. Reference hydrocarbons, cholesterol ($C_{27}H_{45}OH$) and menthol ($C_{10}H_{19}OH$), were also measured for C–H stretch band frequencies and relative integrated intensity factors, $\kappa_{-CH_x}$. For the irradiated VGCF, a band was found to be centered at 2892 $cm^{-1}$, in between a $-CH_3$ symmetric (2873 $cm^{-1}$) and a $>CH_2$ asymmetric (2924 $cm^{-1}$) stretch band, which was assigned to a >CH– stretch band. Relative densities of the $CH_x$ groups, assuming $\kappa_{=CH-}:\kappa_{-CH_3}:\kappa_{>CH_2}:\kappa_{>CH-} = 0.12:2.2:1.1:1.0$, showed that $>CH_2$ decreases in density with increasing the irradiation temperature beyond 1000 K, while >CH– reaches maximum at around 823 K and then decreases. The $-CH_3$ group decreases to a minimum from 623 to 823 K, and increases at above 823 K, indicating that methane forms at around 800 K through abstraction of H from >CH– by free $CH_3$. The density ratio of >CH– to $>CH_2$ reached a maximum at 0.4 at around 800 K, indicating that, in the keV-$H^+$ implantation layer, the implanted H atoms are trapped mainly at $>CH_2$, and subsidiarily at >CH–, and $-CH_3$, at defects, below 900 K. 

*Keywords:* Hydrogen trapping in graphite; Carbon; Methane formation; Chemical sputtering; Graphite; Hydrogen ion irradiation

## 1. Introduction

Graphite is a reference candidate for divertor armors of fusion experimental reactors such as ITER [1]. Trap sites and bond-energies for hydrogen in graphite are essential information for suppression or control of chemical sputtering, recycling and tritium inventory. High-resolution electron energy loss spectroscopy (HREELS) [2] and Fourier-transform infrared absorption spectroscopy (FT-IR), which were successful in semi-quantitative analyses of $sp^2$- and $sp^3$-type CH bondings, were not effective for discrimination of >CH–, $>CH_2$ and $-CH_3$ groups in hydrogen-saturated graphite: resolution is still limited for HREELS [3], or deteriorated for FT-IR due to possible line broadening from residual stress in the thin film specimens on substrates [4].

In the present study, the use of vapor-grown carbon fiber (VGCF) of 'growth-ring' structure [5] of a 200 nm mean diameter resulted in (i) high-resolution C–H stretch band analyses for >CH–, $>CH_2$ and $-CH_3$ groups probably due to the lower irradiation-induced stress compared to that for thin film, and (ii) semi-quantitative treatment of the absorption band intensity because of their angular-independence due to the randomly oriented *c*-axes of the graphite crystallites with respect to both ion and IR-photon beam. For uniform implantation of the VGCF bulk, hydrogen ions of

* Corresponding author. Present address: Department of Reactor Engineering, Energy System Assessment Laboratory, Japan Atomic Energy Research Institute, Naka-gun, Ibaraki-ken 319-11, Japan. Tel.: +81-29 282 6035; fax: +81-29 282 6433; e-mail: gotohy@ruby.tokai.jaeri.go.jp.

0022-3115/99/$ – see front matter 
PII: S0022-3115(98)00853-8

energies 6, 3 and 1 keV were successively irradiated to saturation in this order, simulating keV-$H^+$ irradiation to the graphite basal face.

Band frequencies and intensity factors for $CH_x$ groups, especially for tertiary >CH–, are often found to be contradictory in the literatures [6,7], and were experimentally estimated from high-resolution FT-IR spectra of two reference hydrocarbons: (1) cholesterol, a rather large molecule of a combined alicyclic-branched chain structure to which are bound all four kinds of $CH_x$ groups, =CH–, >CH–, $>CH_2$ and $–CH_3$ of both axial and equatorial configurations; and (2) menthol, a small, combined alicyclic-branched aliphatic chain structure in which both >CH– and equatorial $–CH_3$ groups exist. Semi-quantitative analyses of the $CH_x$ groups within the keV-$H^+$ implantation layer are made as functions of both irradiation temperature and heat-treatment temperature after the irradiations.

## 2. Experimental

### 2.1. Hydrogen irradiation experiments on VGCF

VGCF of 200 nm mean diameter, after heat-treatment at above 3100 K, was mounted on a silicon substrate ($10 \times 10 \times 2$ mm), at densities around several 100 micro-grams/$cm^2$ by dipping Si substrate in a toluen suspension of VGCF and drying it at ambient temperature.

Two series of hydrogen irradiation experiments were made on VGCF/Si by using an ion beam apparatus equipped with a microwave ion source described elsewhere [8]. First isothermal $H^+$ irradiation experiments were done in which mass-separated $H^+$ ion beams of different energies at 6.0, 3.0 and 1.0 keV/H were used at ion fluxes of, $3 \times 10^{14}$, $1 \times 10^{15}$ and $3 \times 10^{15}$ H/$cm^2$ s, respectively, to a fluence of $5 \times 10^{18}$ H/$cm^2$ each. Irradiation temperatures were 373, 623, 823 and 923 K. An Si substrate mounted with VGCF on its front face, was heated at the rear face either with thermal radiation from a resistively heated tantalum heater or, in the higher temperature range, with both thermal radiation and an electron beam accelerated from the heater. The specimen temperature was measured with a W–W80%–Re20% thermocouple element inserted in a hole at the side face of the Si substrate. Immediately after termination of the irradiation, the specimen temperature was decreased to ambient temperature at a typical cooling rate of 6 K/s. Second, isochronal heat-treatment experiments were performed after $H^+$ irradiation at 623 K, in which successive irradiation of $H^+$ ion beams were made at the same conditions for the isothermal experiment at 623 K, followed by in situ heat-treatment at 893, 1000 or 1150 K for 600 s.

### 2.2. FT-IR for reference hydrocarbon molecules

Two reference hydrocarbon molecules were chosen: (1) $C_{27}H_{45}OH$ (Cholesterol Standard, Wako Pure Chemical Industries) and (2) $C_{10}H_{19}OH$ (l-Menthol, 98.0%, Kanto Chemical). To obtain high-resolution FT-IR spectra, the reference material was dissolved in $CCl_4$ in an IR-transparent cell at various concentrations. FT-IR spectra of the reference molecules were recorded in absorbance by using an FTS-40A, Bio-Rad spectrometer with a resolution of 0.5 $cm^{-1}$, aperture diameter set for 0.5 $cm^{-1}$ and MCT ($Hg_{1-x}Cd_xTe$) detector. Data acquisition was made by co-addition of 16 interferograms. High-resolution C–H stretch band spectra were recorded with maximum band absorbance in the range of 0.02–0.06.

### 2.3. FT-IR of $H^+$ irradiated VGCF

The VGCF after the irradiation and/or heat-treatment was removed from the Si substrate, mixed with KBr powder and then molded into a pellet. The FT-IR spectrometer used for the $H^+$ irradiated VGCF analyses was the same as that for the reference molecule analysis, but with a lower resolution of 4 $cm^{-1}$ and aperture diameter set for 1 $cm^{-1}$, due to the lower absorbance of the VGCF specimens. Data acquisition was made by 256 or 1024 co-addition of the interferograms.

### 2.4. Peak separation procedures

The C–H stretching region of the spectra were studied by curve fitting analysis. As a first approximation, linear sloping baselines were used for background subtraction. Band frequencies, FWHM, peak height, combining ratio of Gaussian/Lorentzian distribution were fitted to the experimental envelope by a minimum least squares iterative procedure. In the analyses of the hydrogen-irradiated VGCF spectra, initial values of those parameters were set at expected values referring to reference hydrocarbon data.

## 3. Results

### 3.1. C–H stretch bands observed for cholesterol and menthol

Figs. 1 and 2 show the FT-IR spectra of cholesterol and menthol in the CH stretch band region, respectively, along with the separated bands (dashed lines), through curve fitting, and band assignment. Relative integrated intensity factors, $\kappa_{-CHx}$, for $–CH_x$ group with respect to that for >CH–, were estimated from the integrated absorbance of the separated bands that belongs to each group [9], according to the following equation:

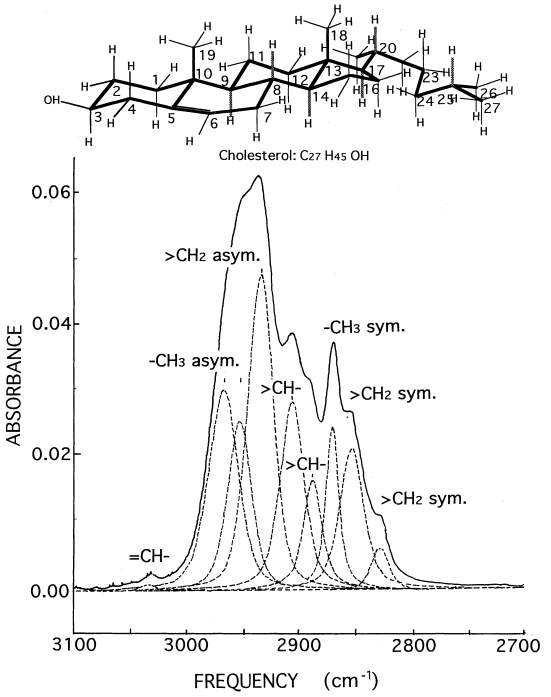


Fig. 1. The FT-IR spectra of cholesterol in the CH stretch band region with the curve-fitting analysis results (dashed lines) and band assignments. The inset shows the molecular structure of cholesterol.

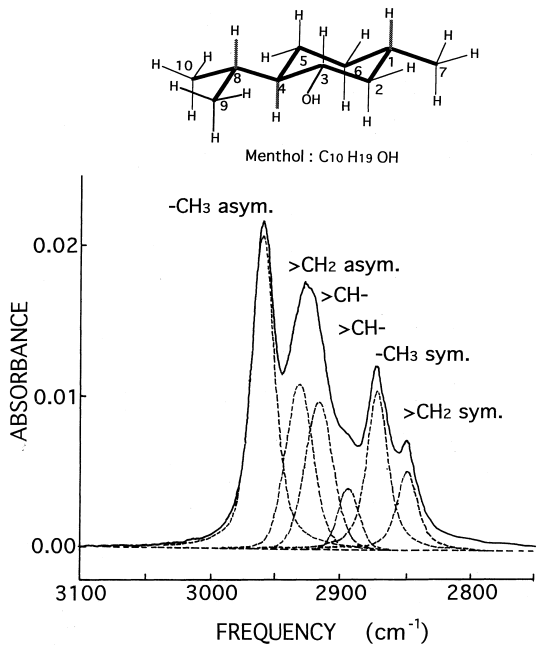


Fig. 2. The FT-IR spectra of menthol in the CH stretch band region with the band separation through curve-fitting and band assignments. The inset shows the molecular structure of menthol.

$$\kappa_{\text{–CH}_x} = \left[\sum_j I_{\text{a CH}_x\, j} / \left(\omega_{\text{CH}_x\, j}\, \zeta_{\text{CH}_x}\right)\right] \Big/ \left[\sum_k I_{\text{a >CH– }k} / \left(\omega_{\text{>CH– }k} \zeta_{\text{>CH–}}\right)\right], \quad (1)$$

where $I_{\text{a CH}_x\, j}$ and $I_{\text{a>CH–}k}$ are absorption area, $\omega_{\text{CH}_x\, j}$ and $\omega_{\text{>CH–}k}$ are band frequencies for $j$th and $k$th C–H stretching absorption bands originating in $\text{CH}_x$ and >CH–, while $\zeta_{\text{CH}_x}$ and $\zeta_{\text{>CH–}}$ are number of $\text{CH}_x$ and >CH– groups per molecule, respectively. Table 1 summarizes the analysis results for cholesterol, and Table 2 summarizes those for menthol.

Relative integrated sensitivity factors, $\kappa_{\text{CH}_x}$, for the $\text{CH}_x$ groups with respect to that of the >CH– group were determined as the averaged values from the cholesterol and the menthol data:

$$\kappa_{\text{=CH–}} : \kappa_{\text{–CH}_3} : \kappa_{\text{>CH}_2} : \kappa_{\text{>CH–}} = 0.12 : 2.2 : 1.1 : 1.0. \quad (2)$$

### 3.2. C–H stretch bands observed for the keV-$H^+$ irradiated VGCF

#### 3.2.1. Irradiation temperature dependence of the CH stretch band spectrum

Fig. 3(a)–(d) shows the selected CH stretch band region observed for VGCF after successive irradiations of 6.0, 3.0 and 1.0 keV $H^+$ ions to saturation at temperatures of 373, 623, 823 and 923 K, respectively. The observed CH stretch band was separated into five or six bands through curve-fitting analyses, referring to the cholesterol and the menthol data. The separated bands (dashed lines), their assignments, the band frequencies, together with residues (solid lines), are indicated in Fig. 3, while the band frequencies, FWHMs and absorption area are listed in Table 3.

Fig. 4 shows the estimated relative density of the $\text{CH}_x$ groups in the implantation layer of VGCF as a function of the irradiation temperature. The density was estimated from the integrated absorbance of the CH stretch bands that belong to the same group, and divided by the relative integrated intensity factor, $\kappa_{\text{–CH}_x}$, determined from the reference molecule data.

#### 3.2.2. Isochronal heat-treatment temperature dependence of the CH stretch bands

Fig. 5(a)–(d) shows the FT-IR spectra from the VGCF after the successive irradiations of 6.0, 3.0 and 1.0 keV $H^+$ ions to saturation at 623 K (a), and then heat-treated for 600 s at temperatures of 893 K (b), 1000 K (c) and 1150 K (d), respectively. The results of band separation (dashed lines), band assignments and frequencies, together with the residues (solid lines), are shown in Fig. 5. From the integrated absorbance due to each $\text{–CH}_x$ group divided by the $\kappa_{\text{–CH}_x}$, the estimated relative number densities of the $\text{CH}_x$ in the hydrogen-ion implanted VGCF are shown as a function of the heat-treatment temperature in Fig. 6.

Table 1
Number of groups per molecule, types of bondings, band frequency, full width at half maximum (FWHM), peak area, $I_{a\ CH_x}$, number of groups relevant to each absorption band, and relative integrated intensity factor, $\kappa_{-CH_x}$, estimated for the CH stretch bands of cholesterol

| Group, $CH_x$ | No. of groups, $\zeta_{CHx}$ | $\kappa_{-CH_x}$ | Mode | Type | No. of relevant groups | Frequency $\omega_{CH_x}$ ($cm^{-2}$) | FWHM ($cm^{-1}$) | Area, $I_{a\ CH_x}$ (%) |
|---|---|---|---|---|---|---|---|---|
| =CH– | 1 | 0.12 | – | Cyclo-hexenic | 1 | 3034 | 19 | 0.27 |
| $–CH_3$ | 5 | 2.1 | Asym. | Equator. Aliphat. | 3 | 2968 | 31 | 18.6 |
| | | 2.1 | Asym. | Axial | 2 | 2953 | 25 | 12.7 |
| | | 2.1 | Sym. | – | 5 | 2870 | 13 | 7.3 |
| $>CH_2$ | 11 | 0.95 | Asym. | – | 11 | 2935 | 28 | 25.5 |
| | | 0.95 | Sym. | Cyclo-hexenic | 10 | 2853 | 25 | 11.0 |
| | | 0.95 | Sym. | Cyclo-hexenic | 1 | 2828 | 18 | 2.2 |
| >CH– | 6 | 1.0 | – | Alicyclic | 4 | 2906 | 25 | 15.0 |
| | | 1.0 | – | Alicyclic | 2 | 2888 | 20 | 7.3 |

Table 2
Number of groups per molecule, types of bondings, mode, band frequency, full width at half maximum (FWHM), peak area, $I_{a\ CH_x}$, number of groups relevant to each band, and relative integrated intensity factor, $\kappa_{-CH_x}$, estimated for the CH stretch bands of menthol

| Group, $CH_x$ | No. of groups, $\zeta_{CHx}$ | $\kappa_{-CH_x}$ | Mode | Type | No. of relevant groups | Frequency $\omega_{CH_x}$ ($cm^{-1}$) | FWHM ($cm^{-1}$) | Adsorption area, $I_{a\ CH_x}$ (%) |
|---|---|---|---|---|---|---|---|---|
| $–CH_3$ | 3 | 2.3 | Asym. | Equator. | 3 | 2959 | 20 | 34.4 |
| | | 2.3 | Sym. | Equator. | 3 | 2871 | 19 | 16.3 |
| $>CH_2$ | 3 | 1.2 | Asym. | Alicyclic | 3 | 2931 | 25 | 18.8 |
| | | 1.2 | Sym. | Alicyclic | 3 | 2848 | 19 | 8.1 |
| >CH– | 3 | 1.0 | – | Alicyclic | 2 | 2915 | 25 | 17.0 |
| | | 1.0 | – | Alicyclic | 1 | 2893 | 18 | 5.3 |

## 4. Discussion

### 4.1. Assignment for the C–H stretch bands

It is commonly accepted that frequencies for asymmetric and symmetric stretch bands of aliphatic $>CH_2$ are at 2920–2926 and 2850–2855 $cm^{-1}$, respectively, while those for $–CH_3$, are at 2960–2970 and 2870–2885 $cm^{-1}$, respectively [10,11].

On the other hand, frequency for the >CH– stretch band reported in the literature can be divided into two groups, 2890 $cm^{-1}$ [6,10], and 2915–2925 $cm^{-1}$ [7,12]. In the present study, those from the branch of the >CH– group in alicyclic structures of cholesterol and menthol were observed at the relatively higher frequencies of 2906 and 2915 $cm^{-1}$, respectively, while those from the branch of the aliphatic chain, at the lower frequencies of 2888 and at 2893 $cm^{-1}$, respectively, with FWHMs of 18–25 $cm^{-1}$. On the other hand, a broad C–H stretch band in the $H^+$ irradiated VGCF, found at 2890–2896 $cm^{-1}$, possessed a much larger FWHM of 31 $cm^{-1}$ when compared to those of the references. From the reference data, the broad bands centered at 2890–2896 $cm^{-1}$ can be assigned to >CH– group probably composed of both alicyclic and branched aliphatic components.

As is shown in Fig. 3(d), with increasing the irradiation temperature above 800 K, new C–H stretch bands at 3007, 3019 and 3031 $cm^{-1}$ appeared, which were assigned to olefinic =CH– in methylcyclohexene-like structures. A 2841 $cm^{-1}$ band also appeared, which coincides very well with that of $>CH_2$ adjacent to =CH– in methylcyclohexene-type hexagonal ring structure [6]. Growth of those bands with increasing irradiation temperature above 823 K indicates that hydrogen detrapping takes place first at >CH–.

### 4.2. Relative number density of the $CH_x$ as a function of temperature

Average integrated intensity factors for =CH–, $–CH_3$, $>CH_2$ and >CH– have been estimated by Fox and Martin for various aliphatic molecular data from dispersion-type spectrometers [6]. The reported value for >CH–, relative to those for =CH–, $–CH_3$, $>CH_2$ is more

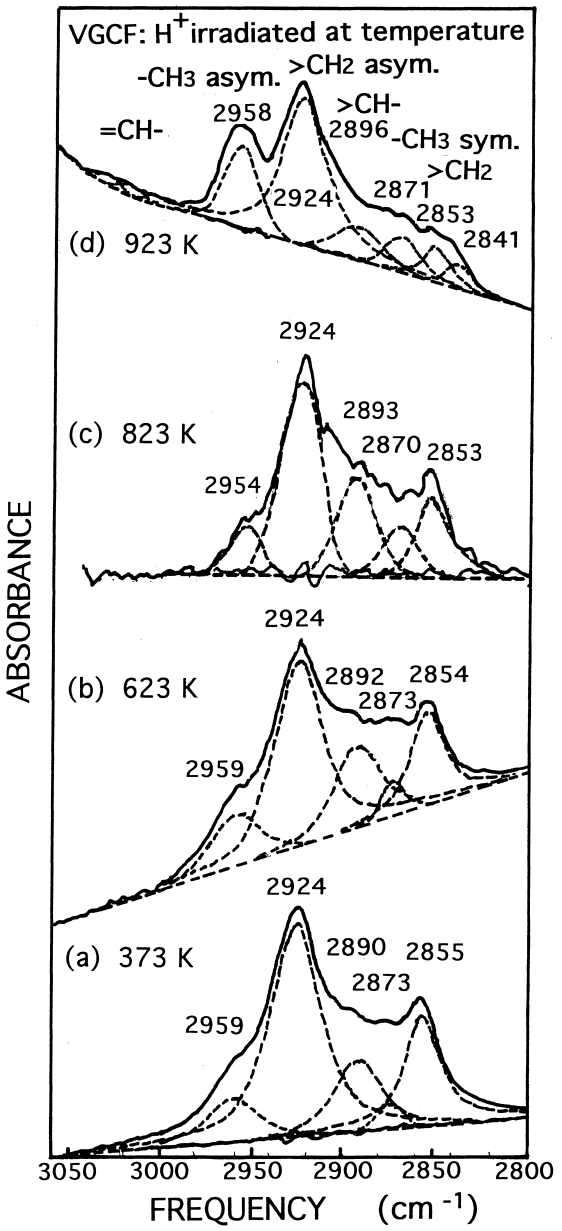


Fig. 3. The FT-IR spectra in the CH stretch band region of the VGCF after successive irradiations of 6.0, 3.0 and 1.0 keV $H^+$ ions to saturation. (a) 373 K, (b) 623 K, (c) 823 K, (d) 923 K. The separated-band assignment, band frequency are indicated at the resolved bands.

than one order of magnitude lower than the present estimated value, probably due to the lower resolution of their spectra or differences in the curve-fitting method used. The present estimated relative integrated intensity factors, especially for >CH–, are not in contradiction with the published data on the IR intensity factor of isobutane [13].

In contrast to the isochronal heat-treatment data (Fig. 6), in which the relative densities of the $CH_x$ group are not largely changed by the heat-treatment below 900 K, the isothermal data (Fig. 4), show that the relative density of the $>CH_2$ groups gradually decreased, while that of the >CH– groups increased, as the irradiation temperature was increased from 500 K to around 800 K. The observed decrease in the relative density of $>CH_2$ compared to that of >CH– can be explained through the structure change of the $H^+$ implantation layer of graphite from aliphatic, i.e. amorphous, to a more graphitic [8,14,15], or to a more alicyclic structure. The density ratio of >CH– to $>CH_2$ in the hydrogen-saturated VGCF was observed to increase to a maximum of 0.4 by increasing the irradiation temperature from 500 to 823 K. A hydrogen trap model can be proposed that implanted hydrogen atoms are trapped at tertiary (>CH–) and secondary ($>CH_2$) carbons, at defects such as vacancies and grain boundary edges, and also as $–CH_3$ bound to tertiary carbons which very likely originated from interstitials.

From both the present isothermal irradiation and isochronal heat-treatment data, it is obvious that, with increasing temperature, first hydrogen atoms trapped at >CH– are detrapped at temperatures above 800–900 K, and then those at $>CH_2$ are detrapped at above 1000 K.

Concerning accuracy in the present estimation of the relative $–CH_3$ group density, due to the much lower density of the $–CH_3$ than that of the $>CH_2$ together with the use of linear sloping background, the accuracy of the estimated $–CH_3$ density is estimated to be at around 50%. Another problem may arise if equatorial $CH_3$ groups bound to carbons of unsaturated bondings with neighboring carbons should exist, that C–H stretch bands of the $–CH_3$ will contribute to the IR absorbance at around 2920 $cm^{-1}$ as well as at 2970 and 2870 $cm^{-1}$ [6]. Such a possibility may exist for the present irradiation experiments above 800 K in which unsaturated bonds are partly formed. In that case, overestimation for $>CH_2$ group density, while underestimation for $–CH_3$ group density could occur. After taking those possibilities into account, it is still obvious in the isothermal irradiation experimental data (Fig. 4), that inverse temperature dependencies exist between the $–CH_3$ and the >CH– in the 600–900 K range, indicating that H atoms trapped at >CH– are abstracted by free $CH_3$ radials which are thermally detrapped from the tertiary carbon lattices above 600–700 K. The increase of $–CH_3$ and the decrease of >CH– above 800 K coincides with the experimental observations that the $CH_4$ formation rate reaches a maximum around 800 K for keV $H^+$ ion irradiation to graphite [16]. The decrease in the methane formation above 800 K is explained through decrease in the >CH– density due to detrapping of H from >CH– above 800 K, which finally leads to release of $H_2$ from the implantation layer.

Table 3
Peak separation results for the FT-IR in the C–H stretching region of the hydrogen irradiated VGCF at irradiation temperatures from 373 to 923 K

| Group, $CH_x$ | $T$ (K) | Mode | Frequency $\omega_{CH_x}$ ($cm^{-1}$) | FWHM ($cm^{-1}$) | Area, $I_{a\ CH_x}$ |
|---|---|---|---|---|---|
| =CH– | 373 | – | – | – | – |
| | 623 | – | – | – | – |
| | 823 | – | – | – | – |
| | 923 | – | 3031, 3019, 3007 | – | 2.9 |
| $–CH_3$ | 373 | Asym. | 2959 | 32 | 10.2 |
| | | Sym. | 2873 | 15 | 2.6 |
| | 623 | Asym. | 2959 | 31 | 12.7 |
| | | Sym. | 2873 | 15 | 3.5 |
| | 823 | Asym. | 2954 | 21 | 8.6 |
| | | Sym. | 2870 | 26 | 9.5 |
| | 923 | Asym. | 2958 | 21 | 16.0 |
| | | Sym. | 2871 | 21 | 7.4 |
| $>CH_2$ | 373 | Asym. | 2924 | 23 | 51.5 |
| | | Sym. | 2855 | 23 | 20.4 |
| | 623 | Asym. | 2924 | 31 | 47.5 |
| | | Sym. | 2854 | 22 | 16.9 |
| | 823 | Asym. | 2924 | 26 | 40.3 |
| | | Sym. | 2853 | 17 | 18.9 |
| | 923 | Asym. | 2923 | 30 | 52.4 |
| | | Sym. | 2853 | 15 | 7.4 |
| | | | 2841 | 16 | 3.9 |
| >CH– | 373 | – | 2890 | 30 | 15.3 |
| | 623 | – | 2892 | 31 | 19.4 |
| | 823 | – | 2893 | 31 | 22.8 |
| | 923 | – | 2895 | 30 | 10.0 |

Since the present FT-IR results strongly indicate the formation of >CH– in the highly graphitic structure within the hydrogen-ion implantation layer of graphite, chemical reactions within the implantation layer can be assumed as gas (molecule or radical)–solid surface ('lateral surfaces') reactions as well as gas phase reactions. The gas phase is composed of $H_2$, H, $CH_x$ ($x = 1$–4), while in the surface layer, active sites such as >CH–, >C–, $>CH_2$, =CH– and =C– exist. Formulations of reaction rate coefficients of the gas–solid surface reactions have been proposed by Frenklach and Wang, modeling the chemical vapor deposition process for diamond film synthesis [17]. According to their methods, reaction rate coefficients for trapping and detrapping of H or $CH_x$ at both $sp^2$- and $sp^3$-type modified graphite surface sites were calculated as a function of temperature as shown in Fig. 7. Methyl group trapped at >C– is expected to be thermally detrapped at temperatures above 650 K, whereas the H remains trapped at >CH–, for temperatures as high as 800 K. Therefore, abstraction of H from >CH– by free $CH_3$ can be inferred to be dominant for methane formation processes above 650 K. Although the rate coefficient for abstraction of $CH_3$ from $>CCH_3$– by H is larger at above 700 K, the free H would be retrapped preferably at an empty >C–. As shown in Fig. 7, H atoms trapped at =CH– at graphite edges are likely not to contribute to the abstraction re-

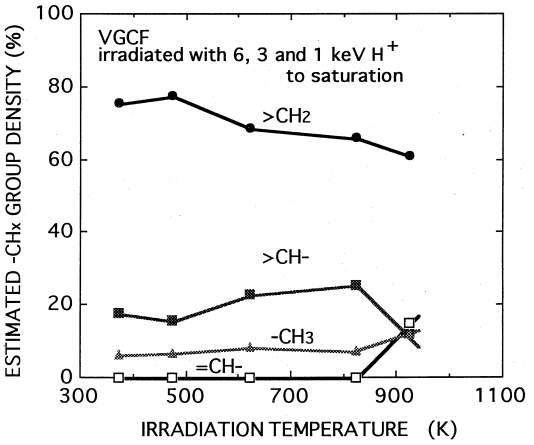


Fig. 4. Estimated relative $–CH_x$ group density in the hydrogen-ion irradiated VGCF as a function of the irradiation temperature. The $–CH_x$ density was estimated from the integrated absorbance of the CH stretch bands that belong to the same group, referring to the relative integrated intensity factor for each group determined from the reference molecular data.

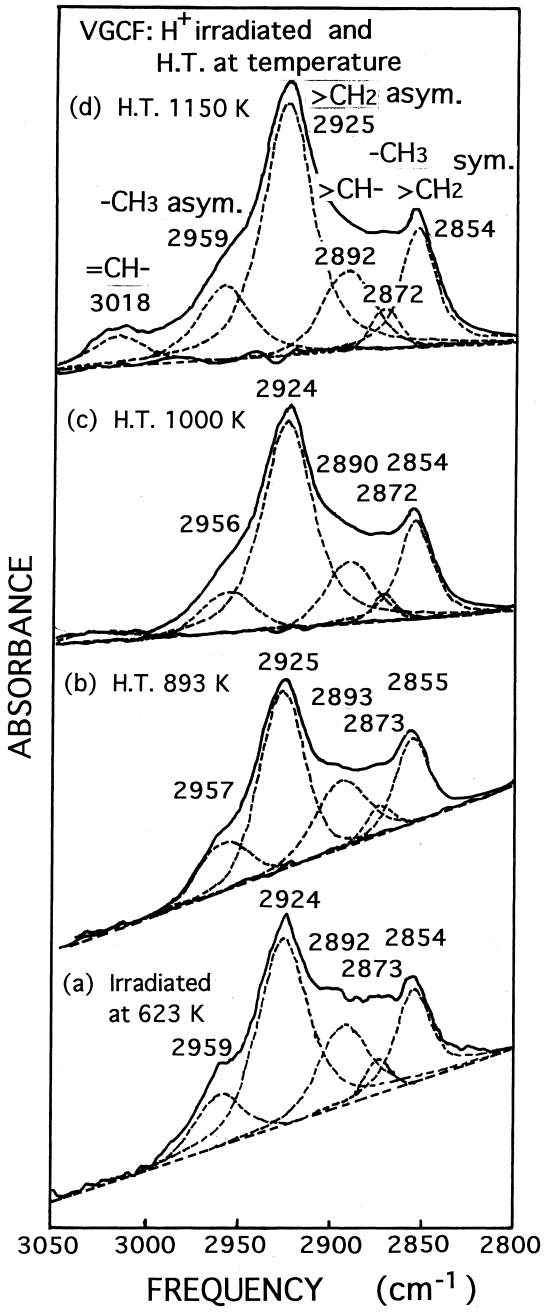


Fig. 5. The FT-IR spectra from the VGCF after successive irradiations of 6.0, 3.0 and 1.0 keV $H^+$ ions to saturation at 623 K, followed by heat-treatment at different temperatures for 600 s: (a) without heat-treatment; (b) after H.T. at 893 K; (c) at 1000 K; (d) at 1150 K.

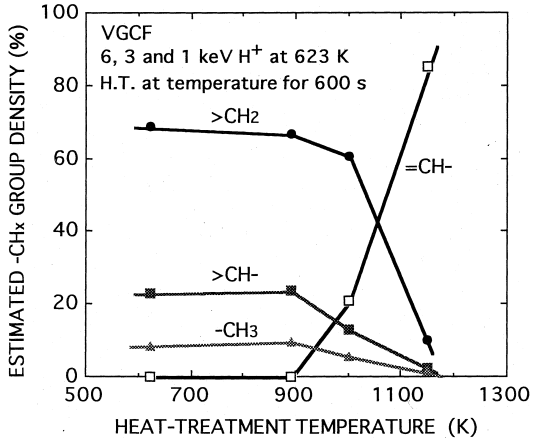


Fig. 6. Estimated relative $CH_x$ density in the hydrogen-ion implanted VGCF with or without the post-irradiation heat-treatment, as a function of the heat-treatment temperature. The $CH_x$ density was estimated from the integrated absorption intensities of the CH stretch bands for each group (Fig. 5), referring to the relative integrated intensity factor determined from the reference molecule data.

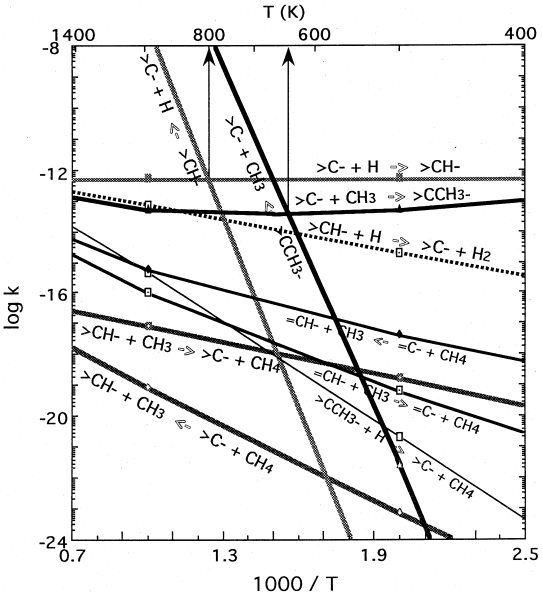


Fig. 7. Arrhenius plots of the calculated rate coefficients for molecular/radical – $H^+$ modified graphite surface reactions, according to the theoretical treatment by Frenklach et al. molecule and radical: H, $H_2$, $CH_x$ ($x=3$, 4), $H^+$-modified graphite surface: $sp^3$:>CH– and >C–; $sp^2$:=CH– and =C–.

action by $CH_3$ because of the higher rate coefficient for its reverse reaction. Thus, the contribution of the activation energy for $CH_4$ formation reaction to the activation energy for methane formation and release is estimated at 0.33 eV from [17]. On the other hand, for $H_2$ formation at just above 800 K the abstraction of the H from >CH– by free H which is detrapped either by thermal or ion-induced processes, is considered to be dominant [18].

In contrast with HREEL results [2], the temperature for the transition from $sp^3$ to $sp^2$ for the present results is 500 K higher than that for the atomic H irradiation experiment on a-C:H films [2]. This difference is considered to be related to the existence of $–CH_3$ or >CH– observed for the keV $H^+$ irradiation experiments. Further studies are necessary on this point.

## 5. Conclusions

From the present FT-IR studies on keV-$H^+$ irradiated VGCF, the following conclusions were deduced:

1. Tertiary >CH– was found to be formed in the hydrogen implantation layer of graphite, along with $>CH_2$, $–CH_3$ and =CH–.
2. Isothermal irradiation and isochronal anneal data showed that hydrogen atoms trapped at >CH– are thermally detrapped above 800 K, while those trapped at $>CH_2$ are thermally detrapped above 1000 K.
3. Methane formation under keV-$H^+$ irradiation is mainly due to abstraction of trapped hydrogen at >CH– by free $CH_3$.
4. The activation energy for the abstraction reaction was inferred to be 0.33 eV from the molecular reaction kinetic data.

## Acknowledgements

The authors are grateful to Dr M. Nakamura, Hitachi Research Laboratory, Hitachi Ltd., for giving valuable advice in acquiring high-resolution FT-IR spectra and the band assignments. The authors are also grateful to Drs Y. Aono and M. Inagaki, Hitachi Research Laboratory, Hitachi Ltd., and also Dr M. Otsuka, Hitachi Works, Hitachi Ltd., for their encouragement in continuing the present study.

## References

[1] ITER, ITER EDA Documentation Series, No.7, IAEA, Vienna, 1996.
[2] A. Horn, A. Shenk, J. Biener, B. Winter, C. Lutterloh, M. Wittmann, J. Küppers, Chem. Phys. Lett. 231 (1994) 193.
[3] J. Biener, A. Shenk, B. Winter, C. Lutterloh, U.A. Schubert, J. Küppers, Surf. Sci. Lett. 291 (1993) L725.
[4] W. Jacob, M. Unger, Appl. Phys. Lett. 68 (1996) 475.
[5] M. Endo, T.C. Chieu, G. Timp, M.S. Dresselhaus, B.S. Elman, Phys. Rev. 28 (1983) 6982.
[6] J.J. Fox, A.E. Martin, Proc. Roy. Soc. A175 (1940) 208.
[7] B. Dischler, E-MRS Meeting, vol. XVII, June 1987, p. 189.
[8] Y. Gotoh, J. Nucl. Mater. 248 (1997) 46.
[9] M.H. Brodsky, M. Cardona, J.J. Cuomo, Phys. Rev. B 16 (1977) 3556.
[10] L.J. Bellamy (Ed.), The Infra-red Spectra of Complex Molecules, Mathuen, London; Wiley, New York, 1958, p. 13.
[11] H.A. Szymanski (Ed.), IR Theory and Practice of Infrared Spectroscopy, Plenum, New York, 1964, p. 208.
[12] P. Couderc, Y. Catherine, Thin Solid Films 146 (1987) 93.
[13] C. Manzanares, I.J. Peng, N. Mina-Camilde, A. Brock, Chem. Phys. 190 (1995) 247.
[14] H. Abe, H. Naramoto, A. Iwase, C. Kinoshita, Nucl. Instrum. Meth. B 127&128 (1997) 681.
[15] K. Niwase, M. Sugimoto, T. Tanabe, F.E. Fujita, J. Nucl. Mater. 155–157 (1989) 303.
[16] W.O. Hofer, J. Roth (Eds.), Physical Processes of the Interactions of Fusion Plasma with Solids, Academic Press, New York, 1996, p. 149.
[17] M. Frenklach, H. Wang, Phys. Rev. B 43 (1991) 1520.
[18] K. Morita, Y. Muto, J. Nucl. Mater. 196–198 (1992) 963.